

Hadronic γ -ray images of Sedov supernova remnants

V. Beshley¹, O. Petruk^{1,2}

¹*Institute for Applied Problems in Mechanics and Mathematics, Naukova St. 3-b, 79060 Lviv, Ukraine*

²*Astronomical Observatory, National University, Kyryla and Methodia St. 8, 79008 Lviv, Ukraine*

Accepted Received ...; in original form ...

ABSTRACT

A number of modern experiments in high-energy astrophysics produce images of supernova remnants (SNRs) in the TeV and GeV gamma-rays. Either relativistic electrons (due to the inverse-Compton scattering) or protons (due to the pion decays) may be responsible for this emission. In particular, the broad-band spectra of SNRs may be explained in both leptonic and hadronic scenarios. Another kind of observational data, namely, images of SNRs, is an important part of experimental information. We present a method to model gamma-ray images of Sedov SNRs in uniform media and magnetic field due to hadronic emission. These γ -rays are assumed to appear as a consequence of meson decays produced in inelastic collisions of accelerated protons with thermal protons downstream of the shock – a model would be relevant for SNRs without firm confirmations of the shock-cloud interaction, as e.g. SN 1006. Distribution of surface brightness of the shell-like SNR is synthesized numerically for a number of configurations. An approximate analytical formula for azimuthal and radial variation of hadronic γ -ray brightness close to the shock is derived. The properties of images as well as the main factors determining the surface brightness distribution are determined. Some conclusions which would be relevant to SN 1006 are discussed.

Key words: ISM: supernova remnants – shock waves – ISM: pion decays – radiation mechanisms: non-thermal – acceleration of particles

1 INTRODUCTION

Cosmic rays (CRs) are an important component of the Universe on different scales, from the Solar System to clusters of galaxies. Supernova remnants (SNRs), sources of galactic CRs, are excellent objects to study magneto-hydrodynamics of nonrelativistic shocks and acceleration of cosmic rays, as well as their mutual influence. Protons and electrons, once heated and accelerated on the shock, produce different types of emission: thermal with maximum intensity in X-rays and nonthermal emission in radio, X-rays and γ -rays. Experiments in high-energy astronomy observe all types of these emission.

Most of galactic cosmic rays are believed to be produced by the forward shocks in supernova remnants (SNRs). A number of indirect evidences favor this expectation. In particular, efficient proton acceleration changes the structure of the shock front and makes plasma more compressible that leads to lower adiabatic index, to increased shock compression ratio and to some observed effects: reduced physical separation between the forward shock and the “contact discontinuity” (or reverse shock) (e.g. Warren et al. 2005) or even protrusions of the ejecta clumps beyond the forward shock (Rakowski et al. 2011); concave shape of the energy spec-

trum (e.g. Reynolds & Ellison 1992); growth of some turbulence modes and amplification of magnetic field in the pre-shock region (e.g. Bell 2004); “blinking” X-ray spots originated from such growth of magnetic field (Uchiyama et al. 2007; Patnaude & Fesen 2007); ordered non-thermal X-ray strips (Eriksen et al. 2011; Bykov et al. 2011).

Nevertheless, there is still lack of direct observational confirmations that protons are accelerated in SNRs to energies which make them responsible for γ -ray emission of SNRs. Broadband spectra of a number of SNRs may be explained either by leptonic or hadronic scenario for γ -ray emission (e.g. SN 1006: Acero et al. 2010). Fermi γ -ray observatory is expected to clarify such ambiguity, at least in bright SNRs (as in RX J1713.7-3946: Abdo et al. 2011). In any case, other kind of experimental information should be studied as well. Namely, the distribution of surface brightness in different bands caused by emission of accelerated particles in SNRs contains wealth of information about properties of CRs and magnetic fields in these objects.

A well known example is the method to estimate the strength of the post-shock magnetic field from the thickness of the radial profiles of X-ray brightness (e.g. Berezhko et al. 2003). Radial structure of the shock front upstream (observed in X-rays) seems to confirm back-reaction of parti-

cles and magnetic field amplification, locally, in SN 1006 (Morlino et al. 2010). A method to derive an aspect angle (between ambient magnetic field and the line of sight) in SNR from the azimuthal variation of the radio brightness is developed in Petruk et al. (2009a) and applied to SN 1006 under assumption of the uniform interstellar magnetic field (ISMF). More detailed consideration of the azimuthal radio profile including the ISMF nonuniformity results in constraints on orientation of ISMF and its gradient around SN 1006 (Bocchino et al. 2011). Radial profiles of the radio brightness may constrain the time evolution of the electron injection efficiency (Petruk et al. 2011a). Spatially resolved spectral analysis of radio and X-ray data (as in SN 1006: Miceli et al. 2009) determines the model, value and surface variation of the electron maximum energy in the SNR (Petruk et al. 2011a).

Properties of the nonthermal images of Sedov SNRs due to radiation of accelerated electrons in radio, X-rays and γ -rays are systematically studied in Reynolds (1998, 2004) and Petruk et al. (2009b, 2011b, Papers I and II respectively). Numerical models for synthesis of maps of adiabatic SNRs in uniform interstellar medium (ISM) and uniform ISMF from basic theoretical principles as well as approximate analytical descriptions are developed in these papers. The main factors determining the azimuthal and radial variation of surface brightness of SNRs are determined. The role of the nonuniform ISM and/or nonuniform ISMF in nonthermal images of SNRs are studied by Orlando et al. (2007, 2011); in particular, gradients of ISMF strength or ISM density result in several types of asymmetries in surface brightness distributions of SNRs in radio, hard X-ray and γ -ray bands. These papers are limited to the test-particle approach because the non-linear theory of diffusive acceleration is not developed for shocks of different obliquity, while the obliquity dependence of various parameters is crucial in image modeling.

In addition to the analysis of SNR images simulated from basic theoretical principles, model-independent methods for SNR images are important. Such method for synthesis of the inverse-Compton γ -ray map of SNR from the radio (or hard X-ray) image and results of the spatially resolved X-ray spectral analysis is developed and applied to SN 1006 in Petruk et al. (2009c). It is found that synthesized inverse-Compton γ -ray image of SN 1006 is in agreement with HESS observations. This fact favors a leptonic scenario for the TeV γ -ray emission of this SNR. Further development of this method allows us to find a new way to constrain the strength of magnetic field in SN 1006 from its nonthermal images (Petruk et al. 2011c).

Though a leptonic scenario for γ -rays from SN 1006 is reasonable and promising (e.g. Petruk et al. 2011a), a hadronic origin cannot be ruled out even in view of the small ISM densities (upper limit is 0.5 cm^{-3} ; e.g. Dubner et al. 2002; Acero et al. 2007), which are consistent with a hadronic scenario (Berezhko et al. 2009; Acero et al. 2010). The shape of the observed spectrum in the TeV γ -ray range better corresponds to the hadronic spectrum rather than to leptonic one (Acero et al. 2010). In order to fit the observed radio, X-ray and gamma-ray emission within the leptonic scenario one needs rather high downstream magnetic field $\approx 30 \mu\text{G}$ (Völk et al. 2008; Petruk et al. 2011a); there is a general thought that such a field can only be pro-

duced by efficiently accelerated cosmic ray proton component.

If TeV γ -rays from SN 1006 is of hadronic origin, then the observed brightness map of this SNR in γ -rays with energy $> 1 \text{ TeV}$ should reflect the distribution of protons with energies $> 2 \text{ TeV}$ which interact with shocked thermal protons inside SNR.

In the present paper, we study this possibility modeling γ -ray images of a Sedov SNR in uniform ISM and uniform ISMF it would have under such scenario. Though we are primarily interested in comparison with SN 1006, our results are general and may be used for analysis of other SNRs.

2 MODEL

2.1 General description

Our model closely restores model used in Papers I and II. Let us consider an adiabatic SNR in uniform ISM and uniform ISMF. Hydrodynamics of the remnant is given by the self-similar Sedov (1959) solutions; in practice, we use their quite accurate approximations in Lagrangian coordinates (Sect. 4 in Petruk 2000). Magnetic field is described following Reynolds (1998); we do not consider amplification of the ambient field (though its role is discussed in Sect. 4). Accelerated protons are described by a number of parameterizations as follows.

At the shock, accelerated protons are distributed with energy E_p as

$$N(E_p) = K_s E_p^{-s+\delta s(E_p)} \exp(-(E_p/E_{p,\max})^\alpha), \quad (1)$$

where N is the differential number density of accelerated protons, $E_{p,\max}$ is the maximum energy of protons, $\delta s(E_p)$ reflects possible concavity of the spectrum shape as an effect of efficient acceleration, s and α are constants, K_s the normalization, index ‘s’ denotes values at the shock. Different theoretical approaches results in different values of α (see references in Reynolds & Keohane 1999; Allen et al. 2008; Orlando et al. 2011; Petruk et al. 2011b) which are between 1/4 and 2. The function $\delta s(E_p)$ varies a bit and very slowly over decades in energy E_p (e.g. Berezhko & Ellison 1999). The emission at some photon energy ε is mostly determined by the narrow range of E_p . Therefore, $\delta s(E_p)$ produces negligible changes to our results and we take it $\delta s(E_p) = 0$.

The maximum energy may vary with obliquity:

$$E_{p,\max}(t, \Theta_o) = E_{p,\max\parallel}(t) \mathcal{E}_{\max}(\Theta_o). \quad (2)$$

where $E_{p,\max\parallel}(t) \propto V(t)^q$, V the shock velocity, q a constant, index “ \parallel ” denotes values at parallel shock, Θ_o is the obliquity angle between the ambient magnetic field and the shock velocity, function $\mathcal{E}_{\max}(\Theta_o)$ is some function.

There are expectations that the efficiency of injection (defined as the ratio of density of accelerated protons to density of all protons) could be most efficient at the parallel shock and progressively depressed toward regions of SNR surface where the shock is perpendicular (Ellison et al. 1995; Völk et al. 2003). In opposite, an analysis of known SNR images presents some hints against such scenario (Fulbright & Reynolds 1990; Orlando et al. 2007); it also reveals that properties of SNR images are similar in isotropic

(no dependence on obliquity) and quasi-perpendicular (injection prefers perpendicular shock) approaches. In our calculations, we use simple parameterizations for obliquity dependence of the injection. Namely, the obliquity dependence of the normalization K_s (which is proportional to the injection efficiency) is parameterized by

$$K_s(t, \Theta_o) = K_{s\parallel}(t) \mathcal{K}(\Theta_o) \quad (3)$$

where $\mathcal{K}(\Theta_o)$ is given by the following formulae where different ‘sensitivity’ to the obliquity angle is given by the parameter Θ_K . The quasi-parallel and quasi-perpendicular injections are represented respectively by

$$\mathcal{K}(\Theta_o) = \exp\left(-(\Theta_o/\Theta_K)^2\right), \quad (4)$$

$$\mathcal{K}(\Theta_o) = \exp\left(-((\Theta_o - \pi/2)/\Theta_K)^2\right). \quad (5)$$

Isotropic injection $\mathcal{K}(\Theta_o) = \text{const}$ may be restored by a large value of Θ_K . Evolution of the injection efficiency may be accounted through $K_{s\parallel} \propto V(t)^{-b}$ where b is a parameter.

The evolution of the proton energy spectrum in the SNR’s interior is considered in the next subsections.

The surface brightness is calculated integrating emissivities along the line of sight within SNR. Hadronic γ -rays appear as a consequence of the neutral pion and η -meson decays produced in inelastic collisions of accelerated protons with *thermal protons downstream of the shock*; the spatial distribution of the target protons inside the volume of SNR is simply proportional to the local plasma density. We use the approach of Aharonian & Atoyan (2000) to calculate the hadronic γ -ray emissivity:

$$q_\gamma(\varepsilon) = 2 \int \frac{q_\pi(E_\pi) dE_\pi}{\sqrt{E_\pi^2 - m_\pi^2 c^4}}, \quad (6)$$

where E_π and m_π are the energy and mass of the neutral pion, the pion emissivity is

$$q_\pi(E_\pi) = \frac{cn_H}{\kappa} \sigma_{pp}(E'_p) N(E'_p), \quad (7)$$

the average energy of protons mostly responsible for creation of pions with energy E_π is

$$E'_p = m_p c^2 + E_\pi / \kappa, \quad (8)$$

$\kappa = 0.17$ (this value accounts also for η -meson production), the cross-section of inelastic collision of a highly-energetic proton with a thermal proton (with negligible energy comparing to the energy of the incident proton) is

$$\sigma_{pp}(E_p) = 28.5 + 1.8 \ln(E_p/1 \text{ GeV}) \text{ mb}. \quad (9)$$

2.2 Proton energy losses due to meson production

In order to synthesize SNR images, we need to know emissivity (6) in each point of the interior and, therefore, to describe evolution of the proton energy spectrum. Relativistic protons lose their energy due to adiabatic expansion and inelastic collisions. Energy losses of protons in the meson production is (Appendix A)

$$-\left(\frac{dE_p}{dt}\right)_{pp} = 3\kappa n_H \sigma_{pp}(E_p) E_{p,\text{kin}}, \quad (10)$$

where c is the speed of light, n_H the number density of the target protons, the factor 3 accounts for the production of π^0 , π^+ and π^- mesons.

The losses due to proton collisions are more significant for larger density of the target protons and higher energy of incident protons. In order to feel then the proton energy losses are effective, let us compare them with the radiative energy losses of electrons

$$-\left(\frac{dE_e}{dt}\right)_{\text{rad}} = \frac{4}{3} \sigma_T c \left(\frac{E_e}{m_e c^2}\right)^2 \left(\frac{B^2}{8\pi}\right) \quad (11)$$

where σ_T is the Thomson cross-section, m_e the mass of electron. The ratio of electron to proton losses is

$$\frac{\dot{E}_{e,\text{rad}}}{\dot{E}_{p,pp}} \simeq 5.0 \frac{B_{\mu\text{G}}^2 E_{e,\text{TeV}}^2}{n_H E_{p,\text{TeV}}}, \quad (12)$$

where we used $\sigma_{pp} \approx 33 \text{ mb}$ (Aharonian & Atoyan 2000), $B_{\mu\text{G}}$ magnetic field in 10^{-6} G , $E_{e,\text{TeV}}$ and $E_{p,\text{TeV}}$ are the energies of electrons and protons measured in 10^{12} eV . One can see that the losses of protons with energy 100 TeV are comparable to losses of electrons with energy 30 TeV in magnetic field $30 \mu\text{G}$, if the number density of target protons is $4 \times 10^4 \text{ cm}^{-3}$ respectively.

2.3 Downstream evolution of the proton energy distribution

Let the energy of proton at the time t_i , when it leaves the region of acceleration, was E_{pi} . Then it is smaller at the present time t (Appendix B),

$$E_p = E_{pi} \mathcal{E}_{ad}(\bar{a})^{\mu(\bar{a})} \mathcal{E}_{pp}(E_p, \bar{a}), \quad (13)$$

because the terms responsible for the adiabatic \mathcal{E}_{ad} and collisional \mathcal{E}_{pp} losses are equal or smaller than unity; $\bar{a} = a/R$, a the Lagrangian coordinate, R the radius of SNR,

$$\mathcal{E}_{ad}(\bar{a}) = \bar{n}(\bar{a})^{1/3}, \quad (14)$$

where $\bar{n} = n/n_s$, index ‘s’ denotes the value immediately post-shock,

$$\mathcal{E}_{pp}(E_p, \bar{a}) = (E_p/1 \text{ GeV})^{1-\mu(\bar{a})} \mathcal{I}(\bar{a}), \quad (15)$$

$\mu(\bar{a})$ and $\mathcal{I}(\bar{a})$ are dimensionless self-similar functions presented in the Appendix B. Close to the shock they behave as (Appendix C)

$$\mathcal{E}_{pp}(\bar{a}) \approx \bar{a}^{\zeta \sigma_{pp}(E_p)}, \quad \mu(\bar{a}) \approx \bar{a}^{-1.8\zeta} \quad (16)$$

where the cross section is in mb, $\zeta = 1.21 \times 10^{-6} t_3 n_{Hs}$, $t_3 = t/1000 \text{ yrs}$, t the age of SNR. One can note that \mathcal{E}_{pp} is effective if the number density of the target protons or/and age of SNR are large.

The energy spectrum of protons downstream of the Sedov shock evolves in a self-similar way (Appendix B)

$$N_p(E_p, \bar{a}, t) = K(\bar{a}, t) E_p^{-s} \mu(\bar{a}) \mathcal{E}_{pp}(E_p, \bar{a})^{s-1} \times \exp\left[-\left(\frac{E_p \bar{a}^{3q/2}}{E_{p,\text{max}} \mathcal{E}_{ad}(\bar{a})^{\mu(\bar{a})} \mathcal{E}_{pp}(E_p, \bar{a})}\right)^\alpha\right]. \quad (17)$$

with $K(\bar{a}, t) = K_s \bar{K}(\bar{a})$, $\bar{K}(\bar{a}) = \bar{a}^{3b/2} \bar{n}(\bar{a})^{1+\mu(\bar{a})(s-1)/3}$. The downstream distribution of relativistic protons are modified mainly by the adiabatic expansion of SNR. Losses due to inelastic collisions affects the distribution only when ζ is not small, that happens when n_{Hs} and/or t are large.

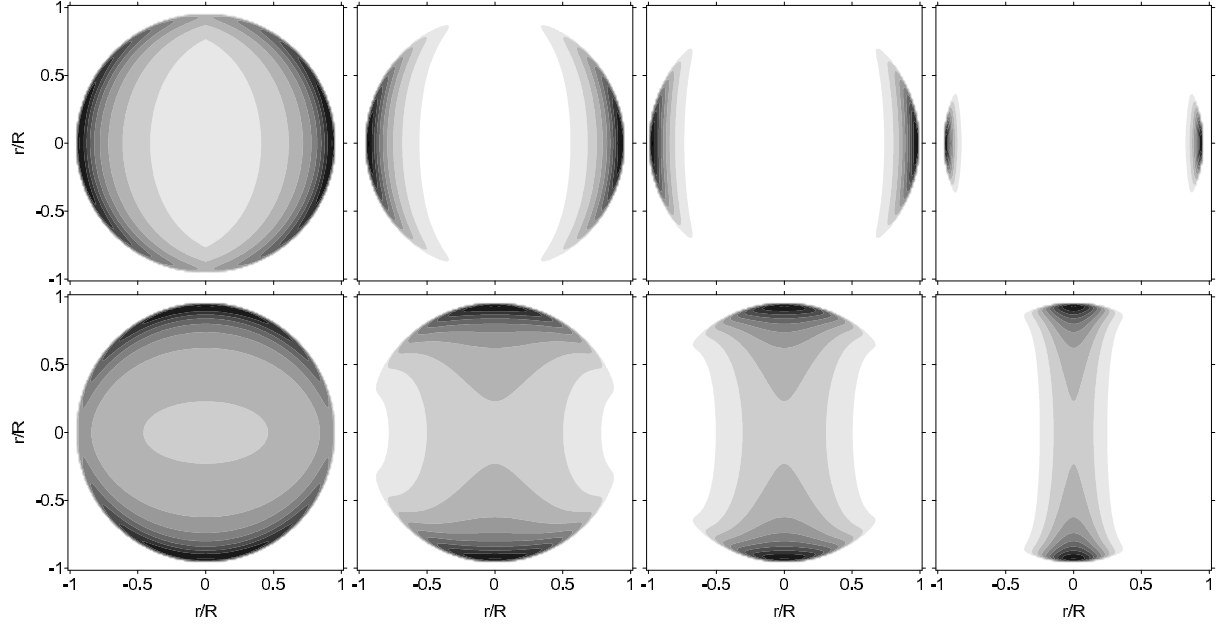


Figure 1. Hadronic γ -ray images of Sedov SNR for different models of injection: quasi-parallel (upper panel) and quasi-perpendicular (lower panel) for an aspect angle $\phi_o = 90^\circ$. Parameter Θ_K is $\pi/2$, $\pi/4$, $\pi/6$, $\pi/12$ (from left). Hereafter, the ISMF is parallel to the horizontal axis and the increment in brightness is $\Delta S = 0.1 S_{\text{max}}$.

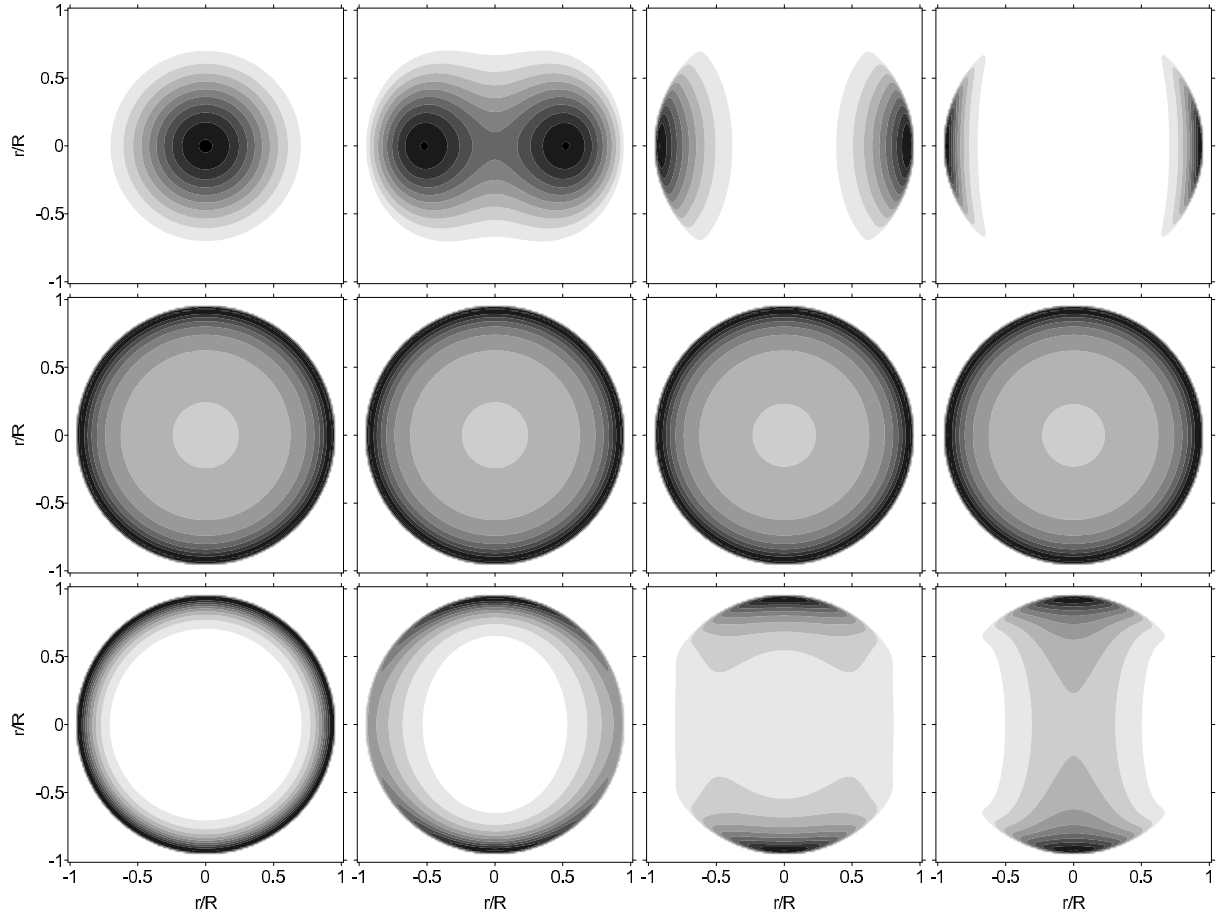


Figure 2. The same as on Fig. 1 for different aspect angles. Models of injection are quasi-parallel (top, $\Theta_K = \pi/6$), isotropic (centre) and quasi-perpendicular (bottom, $\Theta_K = \pi/6$). Aspect angle $\phi_o = 0^\circ$, 30° , 60° and 90° (from left).

3 GENERAL PROPERTIES OF HADRONIC IMAGES. NUMERICAL SIMULATIONS

In order to narrow the parameter space, the images of SNRs in the present section are synthesized using the following set of parameters. Namely, we take $\gamma = 5/3$, $\delta s = 0$, $s = 2$, $\alpha = 1$, K constant in time (i.e. $b = 0$), the energy of γ -rays $\varepsilon = 1$ TeV. The actual representation for $\mathcal{E}_{\max}(\Theta_o)$ used in our calculations is monotonic function which corresponds to the time-limited model of Reynolds (1998) with so called “gyrofactor” $\eta = 1$ (Fig. 1, 2, 5) or $\eta = 5$ (Fig. 3, 4); such form provides $q \approx 0$ and $E_{p,\max}$ at the perpendicular shock to be 2 or 26 times the value at the parallel shock. The age of SNR and the number density are taken $t = 1000$ yrs and $n_{\text{Hs}} = 1 \text{ cm}^{-3}$ except of Fig. 5 where the densities are given in the caption¹. Role of other choices of the above parameters is visible from the approximate formula presented in Sect. 4.

Radio and X-ray synchrotron images of SNRs depends directly on the distribution of magnetic field. Magnetic field affects the TeV γ -ray images of SNR (due to inverse-Compton emission) indirectly, through modification of the downstream evolution of emitting relativistic electrons, namely, the larger the field the larger the radiative losses and, therefore, the thinner the region behind the shock occupied by the electrons able to emit γ -rays in the TeV band (Papers I and II). Magnetic field appears in the hadronic γ -rays only through dependence (if any) of the injection efficiency and the maximum energy on the shock obliquity. Therefore, the azimuthal variation of brightness in such images depends mainly on the two functions: $\mathcal{K}(\Theta_o)$ and $\mathcal{E}_{\max}(\Theta_o)$.

3.1 Different models of injection

Fig. 1 shows how Θ_K affects γ -ray image of SNR it has due to interactions of accelerated protons with thermal protons downstream of the shock. Different dependence of the injection efficiency on obliquity results in two different types of SNR morphology (Fig. 1). Quasi-parallel injection creates the ‘polar-caps’ structure (the lines of ambient magnetic field cross the bright limbs) while the isotropic and the quasi-perpendicular injections are responsible for the ‘barrel-shaped’ remnant (ambient magnetic field is parallel to limbs in this case). Increase of Θ_K results in decrease of the azimuthal width of the limbs due to the progressive lack of accelerated protons.

The role of the aspect angle ϕ_o (between the ambient magnetic field and the line of sight) is shown on Fig. 2. Spherically-symmetric morphology transforms to bilateral one with increasing the angle if the proton injection depends on obliquity.

3.2 Dependence on the maximum energy

The ratio of E_{\max} at the perpendicular and parallel shock is 2 on previous figures. Let the maximum energy of protons increase more rapidly from parallel to perpendicular shock,

¹ parameter really influencing a γ -ray image of SNR is ζ , a product of t and n_{Hs} , Eq. (16).

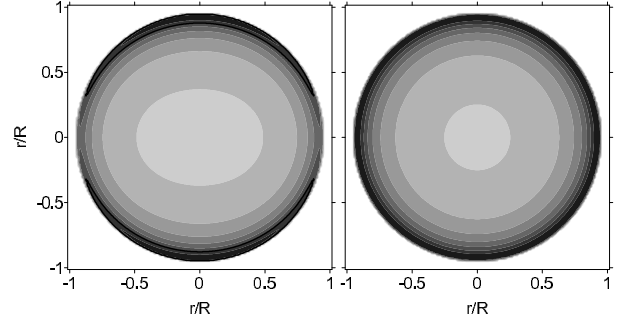


Figure 3. Role of E_{\max} in hadronic γ -ray images of Sedov SNR. $E_{\max\parallel} = 10$ TeV (left, $\epsilon_m = 0.82$), $E_{\max\parallel} = 1000$ TeV (right, $\epsilon_m = 0.0082$). Isotropic injection, $\mathcal{E}_{\max}(\pi/2)/\mathcal{E}_{\max}(0) = 26$, $\alpha = 1$, aspect angle $\phi_o = 90^\circ$.

in particular in 26 times as on Fig. 3. In this case, the azimuthal variation of E_{\max} is in general more prominent.

The thickness of limbs depends on two factors. First, on the ratio $\epsilon_m = E_{p,m}/E_{p,\max\parallel}$ where $E_{p,m}$ is the energy of proton which effectively gives the most contribution to γ -rays with energy ε ; it is given by Eq. (D5); once we are interested in $\varepsilon > 1$ GeV, it may be simplified to

$$E_{p,m}(\varepsilon) = \varepsilon \xi / \kappa = 8.2 \varepsilon. \quad (18)$$

where we used $\xi = 1.4$ (Appendix D). Namely, if $\epsilon_m \ll 1$ then the obliquity variation of the maximum energy does not affect the image of SNR (Fig. 3). Following this conclusion, we would like to note that the role of E_{\max} may be prominent in the analysis of the Fermi observations ($\varepsilon \sim 3$ GeV) only if $E_{p,\max}$ is smaller than ~ 25 GeV that is unreasonable. Therefore, the role of $E_{p,\max}$ may be neglected during analysis of observations in GeV γ -rays.

The second factor which affect the azimuthal thickness of limbs is how quickly the proton energy spectrum $N(E_p)$ ends (given by the parameter α in our model). Fig. 4 demonstrates this effect: the larger α the more rapid decrease of the high-energy end of the proton spectrum and the smaller the azimuthal extension of the limbs.

3.3 Role of density of the target protons

Energy losses of relativistic protons due to collisions with thermal protons are proportional to the density of the target protons, Eq. (10). They were negligible in the calculations presented above because the number density was $n_{\text{Hs}} = 1 \text{ cm}^{-3}$. The collisional losses of protons are important for much higher densities as it is evident from Eq. (16). The role of the pre-shock density in hadronic γ -ray images of SNRs is similar to the role of the magnetic field strength in the hard X-ray images. Namely, the larger the density the higher the collisional losses of accelerated protons and, therefore, the thinner the radial profiles of γ -ray brightness (Fig. 5). This effect may be used for estimation of the target-proton density from thickness of γ -ray rims, once the γ -ray observations reach necessary resolution.

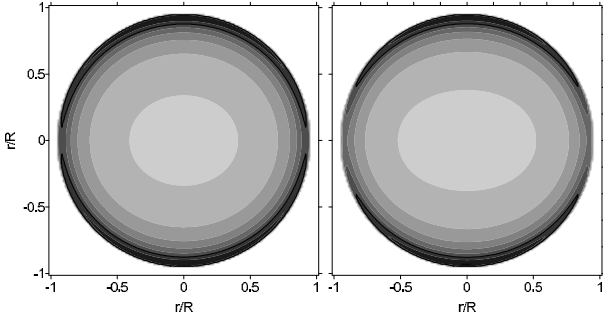


Figure 4. The same as on Fig. 3 for $\alpha = 0.5$ (left) and 2 (right); $E_{\max\parallel} = 10$ TeV.

4 APPROXIMATE ANALYTICAL FORMULA FOR HADRONIC γ -RAY IMAGES

The approximate formulae (valid close to the shock front) for the radial and azimuthal profiles of the surface brightness of Sedov SNR due to leptonic emission (synchrotron radio, X-rays and inverse-Compton γ -rays) are presented in Papers I and II. The same approach is used here to derive an approximation for the surface brightness profiles of hadronic γ -rays arising from internal structures inside adiabatic SNR. Namely (Appendix D),

$$S_p(\varphi, \bar{\varrho}) \propto \varsigma(\Theta_{o,\text{eff}}) \exp \left[- \left(\frac{\epsilon_m}{\mathcal{E}_{\max}(\Theta_{o,\text{eff}})} \right)^\alpha \right] I_{pp}(\Theta_{o,\text{eff}}, \bar{\varrho}) \quad (19)$$

where

$$I_{pp} \approx \frac{1}{\sqrt{1 - \bar{\varrho}^2}} \frac{1 - \bar{\varrho}^{\sigma(\kappa_{pp} + 1)}}{\sigma(\kappa_{pp} + 1)} \times \left[1 - \frac{\epsilon_m^\alpha \psi \alpha}{\mathcal{E}_{\max}^\alpha} \left(1 - \frac{1 - \bar{\varrho}^{\sigma(\kappa_{pp} + 2)}}{1 - \bar{\varrho}^{\sigma(\kappa_{pp} + 1)}} \frac{\kappa_{pp} + 1}{\kappa_{pp} + 2} \right) \right], \quad (20)$$

$\kappa_{pp} = 3b/2 + (5 + s)\kappa_{ad} + 1/\sigma - 1 + \zeta\sigma_{pp}(s - 1)$, $\psi = \kappa_{ad} + \zeta\sigma_{pp} - 3q/2$, $\kappa_{ad} \approx 1$, σ the shock compression ratio, $\bar{\varrho} = \rho/R$. Note, that the azimuthal variation of I_{pp} arises only from obliquity dependence $\mathcal{E}_{\max}(\Theta_{o,\text{eff}})$.

The effective obliquity angle $\Theta_{o,\text{eff}}$, the azimuth φ (measured from the direction of ISMF in the plane of the sky) and the aspect angle ϕ_o are related as

$$\cos \Theta_{o,\text{eff}}(\varphi, \phi_o) = \cos \varphi \sin \phi_o. \quad (21)$$

Approximation (19) is compared with numerical calculations in Appendix D. The formula are rather accurate in description of the brightness distribution close to the shock. It restores all the properties of the surface brightness profiles of Sedov SNR, revealed in the numerical simulations, including dependence on the aspect angle. They are quite useful for qualitative analysis of how different factors affect the hadronic image. They may also be used as a simple quantitative diagnostic tools for hadronic maps of SNRs.

For example, the case when the number density is not high, $\zeta \ll 1$. Then, for known s , the thickness of the γ -ray rim depends mostly on the compression ratio σ and b ; also on α , ϵ_m and q ; the later could be taken zero for an assumption that E_{\max} is limited by the time of acceleration. An opposite case, the product $n_H(t/1000 \text{ yrs}) \geq 10^5$. Then, the term $\zeta\sigma_{pp}$ is dominant in κ_{pp} and ψ and the thickness

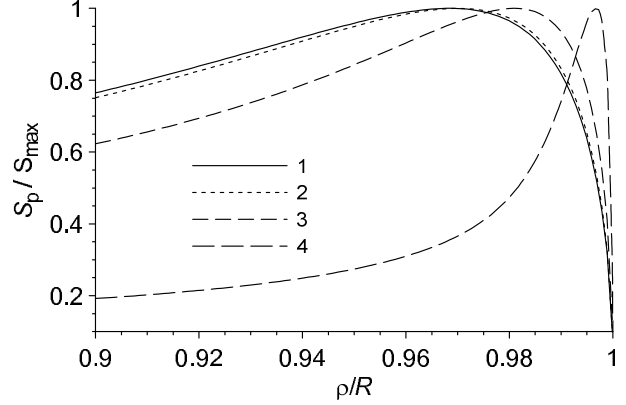


Figure 5. Radial profiles of γ -ray surface brightness due to hadronic emission for different densities n_{Hs} of the target protons: 1 cm^{-3} (line 1), 10^4 cm^{-3} (line 2), 10^5 cm^{-3} (line 3), 10^6 cm^{-3} (line 4). Isotropic injection, $\mathcal{E}_{\max}(\Theta_o) = \text{const}$, $E_{\max\parallel} = 1000$ TeV, $\phi_o = 90^\circ$, azimuth angle (measured from direction of the ambient magnetic field) $\varphi = 0^\circ$. S_{\max} is the peak value of $S_p(\rho)$.

of the γ -ray rim may be used to estimate the post-shock number density.

It is merit to note that our approximate formula reflects also some effects of the non-linear acceleration theory. Namely, in case of efficient proton acceleration, a prominent fraction of the kinetic energy of the shock goes to the relativistic particles. If so, plasma may be described by the adiabatic index γ smaller than $5/3$. In our formula, the adiabatic index appears through the compression ratio σ (Eq. B19) and the parameter κ_{ad} (Eq. C3; though κ_{ad} is close to unity in the range $\gamma = 1.1 \div 5/3$). Features on images are radially thinner for smaller γ . Eventual amplification of magnetic field would be accounted through the larger magnetic field compression ratio; however, this ratio does not appear in our formulae because the hadronic images of SNRs do not depend on the strength of magnetic field.

5 DISCUSSION AND CONCLUSIONS

The spectrum of the TeV γ -rays from SN 1006 may be interpreted as leptonic as hadronic in origin (Acero et al. 2010). The data in the GeV γ -ray range is expected to constrain further this ambiguity. The pattern of surface brightness of SNR also contains important information. In the present paper, we consider possibility that some γ -ray images of SNRs may be hadronic in origin. Namely, we are interested in the images the Sedov SNRs would have if accelerated protons interact with the thermal protons downstream of the shock. The model to synthesize maps of the γ -ray surface brightness of adiabatic SNRs in uniform ISM and uniform ISMF is developed. It includes parameterized description of surface variations of parameters characterizing the injection and acceleration of protons as well as evolution of relativistic protons downstream. The later considers both adiabatic losses of energy and losses due to inelastic collisions. Collisional losses are non-negligible only in case of the large number density of target protons. For example, energy losses of proton with energy 30 TeV due to pp-interactions are comparable to the radiative losses of electrons with the same energy

in magnetic field 30 μG , is the number density of the target protons is $\sim 10^5 \text{ cm}^{-3}$. In case the shock moves in the ambient medium with smaller number density, one can consider only the adiabatic energy losses of accelerated protons to model an image and volume-integrated spectrum of SNR.

The radial thickness of the hadronic γ -ray rim in case of SNR interaction with the large-density ambient material may be used to estimate the density.

The azimuthal variations of the surface brightness of the shell-like adiabatic SNR in hadronic γ -rays is a consequence of the obliquity dependence of the injection efficiency and the maximum energy of accelerated protons. The orientation of the pre-shock magnetic field is the only way the magnetic field influences hadronic images of SNR. If magnetic field is highly turbulent everywhere before the shock of SNR evolving in the uniform ISM then SNR should look as a ring. Nonuniform ISMF (different strength over the SNR surface) does not able to provide any deviation from the ring pattern if information about orientation of ISMF is lost due to turbulence. In contrast, ISM with nonuniform density distribution might provide patterns other than ring, since $K \propto n$. However, it is unlikely that quite symmetrical bilateral structure (as in SN 1006) may appear due to nonuniformity of ISM density because the structure of ISM should be quite special (like a tube, which is not observed around SN 1006).

Bilateral pattern in hadronic image of the shell-like SNR may therefore be considered as a sign of an ordered ambient magnetic field. If so, the limbs are due to azimuthal variation of either \mathcal{K} or \mathcal{E}_{max} . The most contribution to γ -rays with $\varepsilon \sim 1 \text{ TeV}$ gives protons with energy $E_p \sim 8 \text{ TeV}$. Therefore, if $E_{p,\text{max}} \gg 8 \text{ TeV}^2$ then the bilateral pattern of the hadronic TeV image of SNR reveals the variation of the injection efficiency of protons; in fact, Eq. (19) simplifies to $S_p(\varphi) \propto \zeta(\Theta_{\text{o,eff}}(\varphi, \phi_{\text{o}}))$. In this case, the hadronic GeV image has to be the same as TeV γ -ray image (differences in GeV and TeV γ -ray images of SNR are signs of the smaller $E_{p,\text{max}}$ or the contribution from the leptonic emission) and the azimuthal variation of the hadronic γ -ray brightness may be used to derive the obliquity dependence of the proton injection efficiency. Unfortunately, large errors in the present γ -ray data on SN 1006 prevent us from possibility of such an estimate.

ACKNOWLEDGMENTS

The study was partially supported by the program 'Kosmomikrofizyka' of Ukrainian National Academy of Sciences. OP acknowledges F. Bocchino and S. Orlando for hospitality and many useful discussions.

REFERENCES

Abdo A. A., Ackermann M., Ajello M., et al., 2011, *ApJ*, 734, 28
Acero F., Ballet J., Decourchelle A., 2007, *A&A*, 475, 883

² The maximum energy of accelerated protons is typically expected to be up to the knee in the observed cosmic-ray spectrum at 3000 TeV. In particular, the hadronic model of TeV γ -rays from SN 1006 suggests $E_{p,\text{max}} \approx 80 \text{ TeV}$ (Acero et al. 2010).

Acero F., Aharonian F., Akhperjanian A. G., et al., *A&A*, 516, 62
Aharonian F., 2004, *Very High Energy Cosmic Gamma Radiation* (World Scientific)
Aharonian F. A., Atoyan A. M., 2000, *A&A*, 362, 937
Allen G. E., Houck J.C., Sturmer S. J., 2008, *ApJ*, 683, 773
Ballet J. 2006, *Adv. Space Res.*, 37, 1902
Bell A. R., 2004, *MNRAS*, 353, 550
Berezhko E.G., Ellison D. C., 1999, *ApJ*, 526, 385
Berezhko E. G., Ksenofontov L. T., & Völk H. J., 2003, *A&A*, 412, L11
Berezhko E. G., Ksenofontov L. T., & Völk H. J., 2009, *A&A*, 505, 169
Bocchino F., Orlando S., Miceli M., Petruk O., 2011, *A&A*, 531, 129
Bykov A. M., Ellison D. C., Osipov S. M., Pavlov G. G., Uvarov Yu. A., 2011, *ApJ*, 735, L40
Dermer C. D., 1986, *A&A*, 157, 223
Dubner G. M., Giacani E. B., Goss W. M., Green A. J., Nyman L. A., 2002, *A&A*, 387, 1047
Ellison D. C., Baring M. G., Jones F. C., 1995 *ApJ*, 453, 873
Eriksen K. A., Hughes J. P., Badenes C., et al., 2011, *ApJ*, 728, L28
Fulbright M. S., & Reynolds S. P., 1990, *ApJ*, 357, 591
Kelner R. S., Aharonian F. A., Bugayov V. V., 2006, *Phys. Rev. D*, 74, 034018
Miceli M., Bocchino F., Iakubovskiy D., et al., 2009, *A&A*, 501, 239
Mori M., 1997, *ApJ*, 478, 225
Morlino G., Amato E., Blasi P., Caprioli D., 2010, *MNRAS*, 405, L21
Orlando S., Bocchino F., Reale F., Peres G., Petruk O., 2007, *A&A*, 470, 927
Orlando S., Petruk O., Bocchino F., Miceli M., 2011, *A&A*, 526, A129
Patnaude D. J., Fesen R. A. 2007, *AJ*, 133, 147
Petruk O., 2000, *A&A*, 357, 686
Petruk O., Dubner G., Castelletti G., Iakubovskiy D., Kirsch M., Miceli M., Orlando S., Telezhinsky I., 2009a, *MNRAS*, 393, 1034
Petruk O., Beshley V., Bocchino F., Orlando S., 2009b, *MNRAS*, 395, 1467 (Paper I)
Petruk O., Bocchino F., Miceli M., Dubner G., Castelletti G., Orlando S., Iakubovskiy D., Telezhinsky I., 2009c, *MNRAS*, 399, 157
Petruk O., Beshley V., Bocchino F., Miceli M., Orlando S., 2011a, *MNRAS*, 413, 1643
Petruk O., Orlando S., Beshley V., Bocchino F., 2011b, *MNRAS*, 413, 1657 (Paper II)
Petruk O., Kuzyo T., Bocchino F., 2011c, *MNRAS*, accepted (astro-ph: 1109.0831)
Rakowski C. E., Laming J. M., Hwang U., Eriksen K. A., Ghavamian P., Hughes J. P. 2011, *ApJ*, 735, L21
Reynolds S. P., 1998, *ApJ*, 493, 375
Reynolds S. P., 2004, *Adv. Sp. Res.*, 33, 461
Reynolds S.P., Ellison D.C., 1992, *ApJ*, 399, L75
Reynolds S. P., Keohane J. W., 1999, *ApJ*, 525, 368
Schlickeiser R., 2002, *Cosmic Ray Astrophysics* (Springer)
Sedov L.I., 1959, *Similarity and Dimensional Methods in Mechanics* (New York, Academic Press)
Uchiyama Y., Aharonian F. A., Tanaka T., Takahashi T.,

Maeda Y., 2007, *Nature*, 449, 576

Völk H. J., Berezhko E. G., Ksenofontov L. T. 2003, *A&A*, 409, 563

Völk H. J., Ksenofontov L. T., Berezhko E. G. 2008, *A&A*, 490, 515

Warren J. S., Hughes J. P., Badenes C., et al. 2005, *ApJ*, 634, 376

APPENDIX A: ENERGY LOSSES OF PROTONS DUE TO PION PRODUCTION

In order to obtain the energy losses of a “single” proton due to pion production, one needs to integrate the pion source spectra over energies of pions E_π . The pion source spectra is (Schlickeiser 2002)

$$p(E_p, E_\pi) = c n_H E_\pi \frac{d\sigma_{pp}(E_\pi, E_p)}{dE_\pi} H(E_p - E_{th}), \quad (A1)$$

where c , n_H are speed of light and the number density of target protons, $d\sigma_{pp}(E_\pi, E_p)/dE_\pi$ the differential cross-section for the interaction of two protons, E_p the energy of incident proton, H denotes the Heaviside step function and E_{th} the threshold energy of interaction. The energy losses due to inelastic proton collisions is

$$-\left(\frac{dE_p}{dt}\right)_{pp} = 3 \int_0^{E_{\pi, max}} dE_\pi p(E_p, E_\pi), \quad (A2)$$

where the factor 3 accounts for the production of π^0 , π^+ and π^- mesons respectively. In the δ -function approximation, the differential cross section is given by (Dermer 1986a; Mori 1997; Aharonian & Atoyan 2000)

$$\frac{d\sigma_{pp}(E_\pi, E_p)}{dE_\pi} = \sigma_{pp}(E_p) \delta(E_\pi - \kappa E_{p, kin}), \quad (A3)$$

The proton collision losses are

$$-\left(\frac{dE_p}{dt}\right)_{pp} = 3\kappa c n_H \sigma_{pp}(E_p) E_{p, kin}, \quad (A4)$$

where $\kappa = 0.17$ (Aharonian & Atoyan 2000) and therefore $3\kappa = 0.51$ that restores the coefficient of inelasticity $f \approx 0.5$ (Eq. (3.13) in Aharonian 2004).

APPENDIX B: EVOLUTION OF THE PROTON ENERGY SPECTRUM DOWNSTREAM OF THE SHOCK IN SEDOV SNR

We assume that relativistic protons are confined in the fluid elements which advects them from the region of acceleration (Reynolds 1998)³. An individual proton loses energy due

³ This means that we do not account for diffusion in the present consideration. This is the reasonable assumption for protons with $E_p \sim 1$ TeV (and smaller energies) which give most contribution to emission at TeV (GeV) photons respectively, and for the case when the lengthscale of diffusion is proportional to gyroradius. In fact, the gyroradius of the relativistic proton is the same as gyroradius for electron with the same energy; the lengthscale of diffusion for electrons with energy $E_e \sim 1$ TeV (and even for higher energies) are similar or smaller than the lengthscale for advection (Ballet 2006).

to inelastic collisions and adiabatic expansion. Downstream distribution of the target protons is proportional to the density distribution given by Sedov (1959) solution, namely it is $\bar{\rho}(r) = \rho(r)/\rho_s$ where index “s” marks the immediately post-shock value. The pion production losses are given by (A4)

$$-\dot{E}_{p, pp} = 3\kappa c n_{H, s} \bar{\rho}(r) \sigma_{pp}(E_p) E_p \quad (B1)$$

(here, we neglect difference between total and kinetic energies of proton because we are mostly interested in $E_p \gg 1$ GeV). The adiabatic losses are given by (Reynolds 1998)

$$-\dot{E}_{p, ad} = \frac{1}{3} \frac{E_p}{V} \frac{dV}{dt} = -\frac{E_p}{3\bar{\rho}} \frac{d\bar{\rho}}{dt}. \quad (B2)$$

The equation for losses is

$$-\frac{dE_p}{dt} + \frac{E_p}{3\bar{\rho}} \frac{d\bar{\rho}}{dt} = 3\kappa c n_{H, s} \bar{\rho}(r) \sigma_{pp}(E_p) E_p. \quad (B3)$$

In terms of $w = E_p/\bar{\rho}^{1/3}$ (Reynolds 1998), Eq. (B3) is

$$\frac{dw}{dt} = -c_1 \bar{\rho} w \sigma_{pp}(w \bar{\rho}^{1/3}), \quad (B4)$$

where $c_1 = 3 \times 10^{-27} \kappa c n_{H, s}$ cgs.

Let us take the cross section σ_{pp} in the simple form (Aharonian & Atoyan 2000)

$$\sigma_{pp}(E_p) = 28.5 + 1.8 \ln(c_2 E_p) \text{ mb} \quad (B5)$$

where $c_2 = (1 \text{ GeV})^{-1}$.

The solution of this equation is

$$\ln\left(\frac{c_2 E_p}{\bar{\rho}^{1/3}}\right) = \frac{\ln(c_2 E_{pi}) + \ln I}{\mu} \quad (B6)$$

where E_{pi} is the initial proton energy produced on the shock at time t_i ,

$$I(t) = \exp\left[c_1 \int_{t_i}^t q(t') \mu(t') dt'\right], \quad (B7)$$

$$\mu(t) = \exp\left[c_1 \int_{t_i}^t p(t'') dt''\right] \quad (B8)$$

$$p = 1.8\bar{\rho}, \quad (B9)$$

$$q = -\bar{\rho} (28.5 + 1.8 \ln \bar{\rho}^{1/3}). \quad (B10)$$

It follows from (B6) that E_{pi} is related to proton energy E_p at the time of interest t as $E_p = E_{pi} \mathcal{E}_{ad}^\mu \mathcal{E}_{pp}$ where

$$\mathcal{E}_{ad} = \bar{\rho}^{1/3} \quad (B11)$$

represents the adiabatic losses and

$$\mathcal{E}_{pp} = (c_2 E_p)^{1-\mu} I \quad (B12)$$

represents the energy losses due to inelastic collisions.

Self-similarity of the task allows us to write μ and I in terms of the normalized Lagrangian coordinate $\bar{a} = a/R$ rather than in terms of time t . Namely, $I(\bar{a})$ and $\mu(\bar{a})$ are dimensionless functions and, with the use of Sedov (1959) solutions for uniform ambient medium, $dt'/t = (5/2)x^{3/2}dx$ where $x(t') = R(t')/R(t)$, and therefore

$$\mu(\bar{a}) = \exp\left[\zeta \int_{\bar{a}}^1 x^{3/2} p\left(\frac{\bar{a}}{x}\right) dx\right], \quad (B13)$$

$$I(\bar{a}) = \exp \left[\zeta \int_{\bar{a}}^1 x^{3/2} q \left(\frac{\bar{a}}{x} \right) \mu \left(\frac{\bar{a}}{x} \right) dx \right]. \quad (\text{B14})$$

where $\zeta = 5tc_1/2 = 1.21 \times 10^{-6} t_3 n_{\text{Hs}}$, $t_3 = t/1000$ yrs. It is clear from here that \mathcal{E}_{pp} is effective only where the number density of target protons is large, at least $n_{\text{Hs}} \sim 10^6 \text{ cm}^{-3}$.

Thus, relations between energies and energy intervals are

$$E_{\text{pi}} = \frac{E_{\text{p}}}{\mathcal{E}_{\text{ad}}(\bar{a})^{\mu(\bar{a})} \mathcal{E}_{\text{pp}}(E_{\text{p}}, \bar{a})}, \quad (\text{B15})$$

$$\frac{dE_{\text{pi}}}{dE_{\text{p}}} = \frac{\mu(\bar{a})}{\mathcal{E}_{\text{ad}}(\bar{a})^{\mu(\bar{a})} \mathcal{E}_{\text{pp}}(E_{\text{p}}, \bar{a})}. \quad (\text{B16})$$

Let us assume that, at time t_i , a proton distribution has been produced at the shock

$$N(E_{\text{pi}}, t_i) = K_s(t_i) E_{\text{pi}}^{-s} \exp \left[- \left(\frac{E_{\text{pi}}}{E_{\text{p,max}}(t_i)} \right)^\alpha \right], \quad (\text{B17})$$

where α is constant. The conservation equation

$$N(E_{\text{p}}, a, t) = N(E_{\text{pi}}, a, t_i) \frac{a^2 da dE_{\text{pi}}}{\sigma r^2 dr dE_{\text{p}}}, \quad (\text{B18})$$

where

$$\sigma = \frac{\rho_s}{\rho_o} = \frac{\gamma + 1}{\gamma - 1} \quad (\text{B19})$$

is the shock compression ratio (index “o” marks the pre-shock value), and the continuity equation $\rho_o(a) a^2 da = \rho(a, t) r^2 dr$ yield that the energy spectrum evolves downstream as

$$N_{\text{p}}(E_{\text{p}}, a, t) = K(a, t) E_{\text{p}}^{-s} \mu(a) \mathcal{E}_{\text{pp}}(E_{\text{p}}, \bar{a})^{s-1} \times \exp \left[- \left(\frac{E_{\text{p}} \bar{a}^{3q/2}}{E_{\text{p,max}} \mathcal{E}_{\text{ad}}(\bar{a})^{\mu(\bar{a})} \mathcal{E}_{\text{pp}}(E_{\text{p}}, \bar{a})} \right)^\alpha \right] \quad (\text{B20})$$

with $K(a, t) = K_s(t_i) \bar{\rho} \mathcal{E}_{\text{ad}}(\bar{a})^{\mu(\bar{a})(s-1)}$; the evolution of K is self-similar downstream for $K_s \propto V^{-b}$:

$$\bar{K}(\bar{a}) = K(a, t) / K_s(t) = \bar{a}^{3b/2} \bar{\rho}(\bar{a})^{1+\mu(\bar{a})(s-1)/3}. \quad (\text{B21})$$

We note that if the cross section $\sigma_{\text{pp}} \approx \text{const}$ then $\mu = 1$ and $q = \sigma_{\text{pp}} \bar{\rho}$.

APPENDIX C: APPROXIMATIONS FOR EVOLUTION OF SOME PARAMETERS BEHIND THE SHOCK

We interested in approximations of some function χ downstream and close to the shock, in the form

$$\chi(\bar{a}) \approx \bar{a}^\kappa. \quad (\text{C1})$$

By definition

$$\kappa = \left[- \frac{a}{\chi(a)} \frac{\partial \chi(a)}{\partial a} \right]_{a=R} = \left[- \frac{\partial \ln \chi(a)}{\partial \ln a} \right]_{a=R}. \quad (\text{C2})$$

This approach yields for adiabatic losses (Petruk et al. 2011b)

$$\mathcal{E}_{\text{ad}}(\bar{a}) \approx \bar{a}^{\kappa_{\text{ad}}}, \quad \kappa_{\text{ad}} = \frac{5\gamma + 13}{3(\gamma + 1)^2}, \quad (\text{C3})$$

it is valid for $\bar{r} > 0.8$ with error less than few per cent. The value of $\kappa_{\text{ad}} = 1$ for $\gamma = 5/3$ and is close to unity for $\gamma = 1.1 \div 5/3$.

Applying (C2) to Eqs. (B13) and (B14) one obtains:

$$\mu(\bar{a}) \approx a^{-1.8\zeta}, \quad I(\bar{a}) \approx a^{28.5\zeta}. \quad (\text{C4})$$

With these approximations, Eq. (B12) are approximately

$$\mathcal{E}_{\text{pp}}(E_{\text{p}}, \bar{a}) \approx \bar{a}^{\zeta \sigma_{\text{pp}}(E_{\text{p}})} \quad (\text{C5})$$

where the cross section is in units of mb and we used the property $x^{1-\bar{a}^{-z}} \approx \bar{a}^{z \ln(x)}$ which is valid for $\bar{a} \approx 1$. Approximation (C5) is independent of the adiabatic index γ .

APPENDIX D: APPROXIMATE FORMULA FOR PROFILES OF THE HADRONIC SURFACE BRIGHTNESS OF SEDOV SNR

D1 Derivation of the formula

1. The γ -ray emissivity due to meson decays is (Aharonian & Atoyan 2000)

$$q_\gamma(\varepsilon) = 2 \int_{E_{\pi, \min}(\varepsilon)}^{\infty} \frac{q_\pi(E_\pi) dE_\pi}{\sqrt{E_\pi^2 - m_\pi^2 c^4}} \frac{\text{photons}}{\text{cm}^3 \text{ s eV}}, \quad (\text{D1})$$

the pion emissivity

$$q_\pi(E_\pi) = \frac{cn_{\text{H}}}{\kappa} \sigma_{\text{pp}}(E_{\text{p}}') N(E_{\text{p}}'). \quad (\text{D2})$$

On average, energy transferred from protons to pions is $E_\pi = \kappa E_{\text{p,kin}}$, where $\kappa = 0.17$ accounts also for contribution from η -mesons; therefore an average energy of protons mostly responsible for creation of pions with energy E_π is

$$E_{\text{p}}' = m_{\text{p}} c^2 + E_\pi / \kappa. \quad (\text{D3})$$

The minimum energy of pion to create photon is

$$E_{\pi, \min} = \varepsilon + m_\pi^2 c^4 / 4\varepsilon. \quad (\text{D4})$$

Substitution (D4) into (D3) results in expression for $E_{\text{p, min}}'$, an average minimum energy of proton to create photon with energy ε .

Let us introduce an effective energy of protons $E_{\text{pm}}(\varepsilon) = \xi E_{\text{p, min}}'(\varepsilon)$ which gives most contribution to γ -rays with energy ε :

$$E_{\text{pm}}(\varepsilon) = \frac{\xi}{\kappa} \left(\varepsilon + \frac{m_\pi^2 c^4}{4\varepsilon} + \kappa m_{\text{p}} c^2 \right) \quad (\text{D5})$$

and re-write Eq. (D1) in the form

$$q_\gamma(\varepsilon) = \frac{2cn_{\text{H}}}{\kappa} \sigma_{\text{pp}}(E_{\text{pm}}) N(E_{\text{pm}}) F(\varepsilon, \xi) \quad (\text{D6})$$

where

$$F(\varepsilon, \xi) = \int_{E_{\text{p, min}}'(\varepsilon)}^{\infty} \frac{\sigma_{\text{pp}}(E_{\text{p}}') \frac{N(E_{\text{p}}')}{\sigma_{\text{pp}}(\xi E_{\text{p, min}}'(\varepsilon)) \frac{N(\xi E_{\text{p, min}}'(\varepsilon))}{\sqrt{(E_{\text{p}}' - m_{\text{p}} c^2)^2 - m_\pi^2 c^4 / \kappa^2}} dE_{\text{p}}'}{dE_{\text{p}}'}. \quad (\text{D7})$$

$F(\varepsilon, \xi) \approx 1$ is provided by the values $\xi = 1.42, 1.40, 1.44$ for $s = 2, 1.8, 2.2$ respectively, in a wide range of E_{p} (Fig. D1).

To the end, Eq. (D6) becomes

$$q_\gamma(\varepsilon) \approx \frac{2cn_{\text{H}}}{\kappa} \sigma_{\text{pp}}(E_{\text{pm}}) N(E_{\text{pm}}) \quad (\text{D8})$$

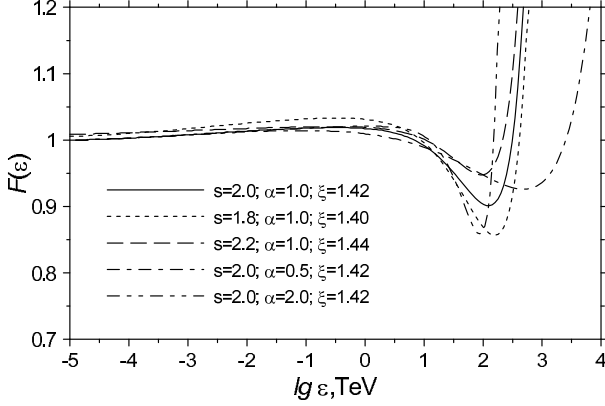


Figure D1. Function $F(\varepsilon)$, Eq. (D7), for few sets of parameters. $E_{p,\max} = 10^{15}$ eV. Rapid deviation the function from unity at energies above $\varepsilon \sim 0.1E_{p,\max}$ corresponds to the rapid decrease of γ -ray emissivity.

We assume that, close to the shock front, the cross section $\sigma_{pp} \approx \text{const}$. The distribution of target thermal protons is proportional to the plasma density, $n_H \propto \bar{n}(\bar{a})$. Therefore, Eq. (D8) may approximately be represented with

$$q_\gamma(\varepsilon) \propto \bar{n}(\bar{a})N(E_{p,m}, \bar{a}). \quad (\text{D9})$$

2. The energy of protons E_p in a given fluid element at present time was $E_{p,i}$ at the time this element was shocked; they are related with (B15). The behavior of the factors \mathcal{E}_{ad} and \mathcal{E}_{pp} close to the shock is given by Eqs. (C3) and (C5). The distribution $N(E_p)$ is therefore approximately

$$N(E_p, \Theta_o) \propto \mathcal{K}(\Theta_o) \bar{K}(\bar{a}) E_p^{-s} \bar{a}^{\psi_2} \times \exp \left[- \left(\frac{E_p \bar{a}^{-\psi}}{E_{p,\max,\parallel} \mathcal{E}_{\max}(\Theta_o)} \right)^\alpha \right]. \quad (\text{D10})$$

where $\psi_2(E_p) = \zeta \sigma_{pp}(s-1)$,

$$\psi = \kappa_{ad} + \zeta \sigma_{pp} - 3q/2 \quad (\text{D11})$$

and we use $\mu = 1$ for $\sigma_{pp} \approx \text{const}$.

3. An ‘effective’ obliquity angle $\Theta_{o,\text{eff}}$ is related to the azimuthal angle φ and the aspect angle ϕ_o as (Papers I and II)

$$\cos \Theta_{o,\text{eff}}(\varphi, \phi_o) = \cos \varphi \sin \phi_o \quad (\text{D12})$$

where the azimuth is measured from the direction of ISMF in the plane of the sky.

The surface brightness of SNR is

$$S(\bar{\varrho}, \varphi) = 2 \int_{\bar{a}(\bar{\varrho})}^1 q_\gamma(\bar{a}) \frac{\bar{r} \bar{r}_{\bar{a}} d\bar{a}}{\sqrt{\bar{r}^2 - \bar{\varrho}^2}}. \quad (\text{D13})$$

where $\bar{\varrho}$ is distance from the centre of the SNR projection, $\bar{r}_{\bar{a}}$ is the derivative of $\bar{r}(\bar{a})$ in respect to \bar{a} . With the use of Eqs. (D9) and (D10), the variation of the meson-decay γ -ray brightness is approximately

$$S_p \propto \varsigma(\Theta_{o,\text{eff}}) \exp \left[- \left(\frac{\epsilon_m(\varepsilon)}{\mathcal{E}_{\max}(\Theta_{o,\text{eff}})} \right)^\alpha \right] I_{pp}(\Theta_{o,\text{eff}}, \bar{\varrho}) \quad (\text{D14})$$

where $\epsilon_m = E_{p,m}/E_{p,\max,\parallel}$,

$$I_{pp} = \int_{\bar{a}(\bar{\varrho})}^1 \frac{\bar{n} \bar{K} \bar{a}^{\psi_2} \bar{r} \bar{r}_{\bar{a}} d\bar{a}}{\sqrt{\bar{r}^2 - \bar{\varrho}^2}} \exp \left[- \frac{\epsilon_m^\alpha}{\mathcal{E}_{\max}^\alpha} (\bar{a}^{-\alpha\psi} - 1) \right]. \quad (\text{D15})$$

4. Let us approximate I_{pp} . Close to the shock front, the density distribution is

$$\bar{n} \approx \bar{a}^{3\kappa_{ad}} \quad (\text{D16})$$

and Eq. (B21) yields therefore

$$\bar{K}(\bar{a}) \approx \bar{a}^{\kappa_{ad}(2+s)+3b/2}. \quad (\text{D17})$$

In addition (Petruk et al. 2011b): $\bar{r}_{\bar{a}} \approx (1/\sigma) \bar{a}^{1/\sigma-1}$, $a \approx r^\sigma$, $\exp(-q_*(a^{-\alpha\psi} - 1)) \approx 1 - q_* \alpha \psi (1 - a)$ and

$$\frac{\bar{r}}{\sqrt{\bar{r}^2 - \bar{\varrho}^2}} \approx \frac{1}{\sqrt{1 - \bar{\varrho}^2}}. \quad (\text{D18})$$

The integral of interest is therefore

$$I_{pp}(\varphi, \bar{\varrho}) \approx \frac{1}{\sqrt{1 - \bar{\varrho}^2}} \frac{1 - \bar{\varrho}^{\sigma(\kappa_{pp}+1)}}{\sigma(\kappa_{pp}+1)} \times \left[1 - \frac{\epsilon_m^\alpha \alpha \psi}{\mathcal{E}_{\max}^\alpha} \left(1 - \frac{1 - \bar{\varrho}^{\sigma(\kappa_{pp}+2)}}{1 - \bar{\varrho}^{\sigma(\kappa_{pp}+1)}} \frac{\kappa_{pp}+1}{\kappa_{pp}+2} \right) \right]. \quad (\text{D19})$$

where

$$\kappa_{pp} = \frac{3b}{2} + (5+s)\kappa_{ad} + \frac{1}{\sigma} - 1 + \zeta \sigma_{pp}(s-1). \quad (\text{D20})$$

The formula Eq. (D14) gives us the possibility to approximate both the azimuthal and the radial brightness profile for $\bar{\varrho}$ close to unity.

D2 Accuracy of the approximation

Fig. D2 demonstrates accuracy of the approximation (D14) (upper and lower panels for azimuthal, radial profiles). Our calculations shows that this approximation may be used, with errors less than $\sim 20 \div 30\%$, in the range of $\bar{\varrho}$ from 0.9 to 1, for azimuth φ where $\varepsilon/E_{p,\max} \leq 0.5, 50, 0.2$ for $\alpha = 1, 0.5, 2$ respectively (Fig. D1). Accuracy of approximation is higher for smaller Θ_K (because the injection term dominates in the azimuthal variation of the brightness) and for smaller variations of \mathcal{E}_{\max} (the role of \mathcal{E}_{\max} becomes however less prominent for smaller ratio ε/E_{\max}).

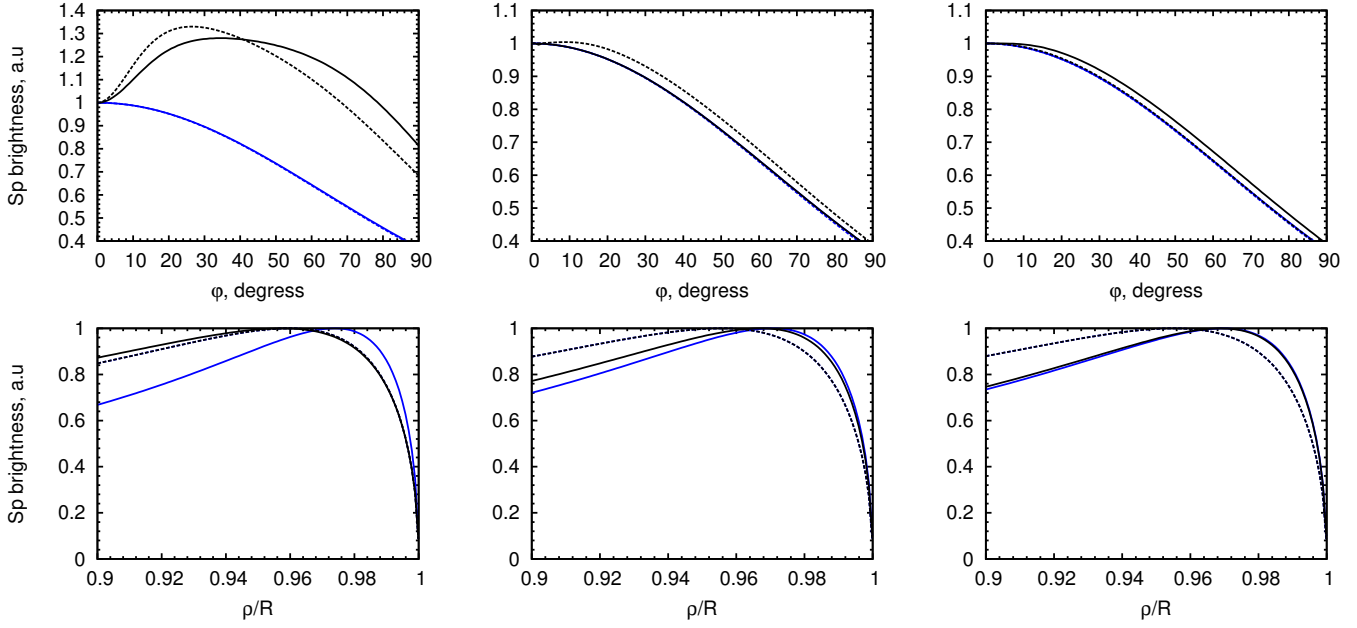


Figure D2. Azimuthal (upper panels) and radial (lower panels) profiles of the hadronic γ -ray surface brightness S_p (solid lines) and their approximations (D14) (dashed lines). Calculations are done for $\phi_0 = 90^\circ$, quasi-parallel injection with $\Theta_K = \pi/2$, other parameters are the same as in Sect. 3. Models of E_{\max} : blue line – $\mathcal{E}_{\max} = \text{const}$; black line – the smooth monotonic variation which provide the variation of \mathcal{E}_{\max} in 3.3 times with azimuth (actual representation used is the time-limited model of Reynolds (1998) with $\eta = 1.5$). The ratio of the photon energy to the maximum proton energy is $\varepsilon/E_{p,\max} = 0.1$ (left), $\varepsilon/E_{\max} = 0.01$ (middle), $\varepsilon/E_{\max} = 0.001$ (right).